Journal of Marine Science and Application (2024) 23: 900-913
https://doi.org/10.1007/s11804-024-00409-2

RESEARCH ARTICLE

Adaptive Path-Following Control for Displacement Vessels at any Loading Conditions Under Ocean Disturbances

Ali Hasanvand[1] **and Mohammad Saeed Seif**[1]

Received: 01 February 2024 / Accepted: 12 April 2024

Abstract
Challenges associated with path-following control for commercial displacement vessels under varying loading and draught conditions are addressed in this study. Adaptive control with the adaptation law technique is used to mitigate the adverse effects of uncertainty and unmodeled parameters on path-following, particularly in the presence of ocean disturbances. The proposed adaptive path-following control estimates the effect of unmodeled parameters and dynamic behavior by the state estimator. Then, the proposed structure adjusts the gains of the L1 controller. The indirect L1 control is used in the main controller, and stability proof is provided based on Lyapunov theory. The adaptive path-following control is proposed for the underactuated-very large crude carrier 2 (VLCC2) as a benchmark vessel. Hydrodynamic coefficients for full load and ballast conditions are determined using empirical formulas. Simulations are conducted in these loading conditions, accounting for a two-knot ocean current, two-knot wind, and waves up to sea state 5. Results highlight that the fixed structure, such as the PID controller, fails to deliver satisfactory performance due to significant variations in the vessel's mass, inertia, and draught. By contrast, the adaptive path-following control demonstrates robustness under varying conditions by effectively estimating the vessel's unmodeled parameters.

Keywords Full scale; Ballast and full load; Adaptive path-following; Model reference; Ocean disturbances

1 Introduction

Marine transportation plays a crucial role in global trade, moving a massive amount of goods across the world's oceans each year. It accounts for approximately 80%–90% of global trade, transporting over 10 billion tons of containerized, solid, and liquid bulk cargo annually (Schnurr and Walker, 2019). The study of cost reduction and enhancement of the performance of maritime fleets has gained considerable interest from researchers. Therefore, the development and expansion of intelligent systems can boost capabilities, reduce costs, enhance safety, and improve transportation service quality in maritime lines.

Article Highlights

- Adaptive structure has had effective performance relative to fixed structure under uncertainties.
- Traditional controller under ocean disturbances cannot track desired path for displacement vessels.
- Energy consumption and actuator usage in adaptive structure is 0.4 times fixed structure under uncertainties.

✉ Mohammad Saeed Seif
Seif@sharif.edu

[1] Department of Mechanical Engineering, Sharif University of Technology, Tehran 11155-9567, Iran

Path-following control systems are intelligent systems designed for many applications, such as underwater exploration and extraction (Pastore and Djapic, 2010), environmental data collection, and research (Švec et al., 2014). The main task of a motion control system is to maintain the vessel in a specific position and course. Although other missions may be considered, the main task is to control the position and course (Yuh et al., 2011). Marine vessel motion control systems are primarily categorized into two principal categories: dynamic positioning (DP) and path-following. The DP system is tasked with controlling the three motions of the vessel's surge, sway, and yaw, whereas path-following focuses on controlling the forward speed and heading (Abril et al., 1997).

The path-following control system consists of three fundamental components: guidance, navigation, and control, which operate in a continuous interconnection (Liu et al., 2016). The navigation system estimates the instantaneous position, the guidance system generates path planning and path re-planning, and the control system provides appropriate commands to actuators to steer the vehicle (Hasanvand and Seif, 2023). Any defects within these components can result in disruption and inappropriate performance of the entire system. The intelligent motion control system generally involves challenges that must be thoroughly examined and addressed prior to implementation on real-scale ves-

sels. The degree of freedom of the control system is a prominent limitation. While some marine vehicles are fully-actuated (Feemster and Esposito, 2011; Wondergem et al., 2010), commercial vessels are often equipped with two main thrusters (Majohr and Buch, 2006; Sharma and Sutton, 2012) or are designed with a single thruster and rudder (Breivik et al., 2008; Sonnenburg and Woolsey, 2013); thus, they are considered underactuated. Underactuated vessels lack direct maneuvering capability in the sway direction. The capabilities of the actuators directly impact path-following control and can be enhanced through geometric characteristic optimization (Hasanvand and Hajivand, 2019; Hasanvand et al., 2021).

Often, a fault or sensor-denied event can occur during endurance. Therefore, some studies have focused on faults. GPS-denied faults are among the most common faults in path-following control. However, a significant number of vessels rely on the global positioning system (GPS) for localization in both positioning methods. Nevertheless, the GPS-based system may not be accessible in some cases, necessitating the consideration of specialized measures (Leslie et al., 2022). A unique visual servo swarming method for a fleet of manned-unmanned surface vehicles (MUSVs) was proposed that incorporates visibility maintenance, swarm aggregation, collision avoidance, and velocity matching (Wang et al., 2023). A swarm of unmanned surface vehicles (USVs) with unknown inertia masses, internal dynamics, and external disturbances can cooperate with a manned surface vehicle, resulting in flexible collective behavior in GPS-denied environments.

While a limited number of studies on the design of intelligent control systems for commercial displacement vessels have been conducted, the majority of research has focused on small-scale USVs. A research review concerning control approaches for USVs is beneficial, given the inherent dynamic similarities among these vessel types. In underactuated marine vehicles, a path-following control system focuses on regulating the speed and direction of the vessel. PID controllers have traditionally served as the primary and widely adopted method for managing the motions of these vessels (Moradi and Katebi, 2001). However, challenges may arise owing to the nonlinear nature of surface vessel dynamics; these difficulties can be addressed by employing more advanced control structures, such as PID-fuzzy controllers (Talha et al., 2017).

We review some studies on path-following control for surface vessels. The Euler approach suggested an active disturbance rejection control for ship path-following (Zhang et al., 2022). The initial three degrees of freedom position control is converted into the one degree of freedom heading control using a backstepping method, constructing the virtual heading angle. An improved "dynamic virtual ship" guidance algorithm and an energy-efficient ship route following a controller are developed by combining nonlinear feedback with adaptive backstepping (Zhao et al., 2023). A backstepping strategy introduced a nonlinear observer defined by an exponential function, which transforms path-following into heading control (Liu et al., 2023). The model predictive control (MPC) method is used as a heading controller to handle the rudder optimization. Optimal usage of actuators is critical in vessel operations because the cost is directly influenced. However, continuous actuator usage leads to increased energy consumption, which is undesirable. The design of optimal controllers, namely, LQR (Lefeber et al., 2003) and MPC (Chowdhury and Schwartz, 2022) in this domain can be highly effective in optimizing the actuator usage. In advance procedures, reinforcement learning can improve the performance of the control system in some conditions. Therefore, optimal tracking control of an unknown unmanned surface vehicle has been investigated by reinforcement learning (Wang et al., 2020). Moreover, an autonomous pilot framework with waypoint generation, path smoothing, and policy direction of a USV in congested waters is built for the first time by naturally integrating path planning and tracking. An elite-duplication GA (EGA) approach is developed by adding elite and diversity operations to the genetic algorithm (GA) to produce sparse waypoints in a limited space in the best possible method (Wang et al., 2021).

The uncertainty parameters in the path-following control of commercial vessels pose a challenge in designing the proposed system. Advanced control techniques, such as H_∞ control (Zhao et al., 2022), sliding mode control (Liu et al., 2014a; 2014b), and neural network training (Pan et al., 2013), can be utilized to mitigate the impact of uncertainty parameters. One of the well-known approaches to overcoming the uncertainties in vessel dynamics is the use of adaptive control structures. For instance, a study used an adaptive backstepping controller to mitigate the adverse effect of unknown disturbances and parameters (Chen et al., 2012). Another research focused on an adaptive sliding mode controller for a multi-input, multi-output USV based on the Lyapunov function (Faramin et al., 2019). A nonlinear model and time-varying parameters devised an adaptive path-following controller for a ship (Liu and Chu, 2020). Diverse control methodologies, such as optimal adaptive control and adaptive sliding mode control (Feemster and Esposito, 2011; Ding et al., 2013; Annamalai et al., 2014), have improved the control signal robustness in the autopilot system for ships and USVs, particularly under uncertain conditions. Uncertainty in position and orientation estimation poses an additional challenge in path-following control systems due to measurement sensor limitations. The use of an observer to estimate system states can notably enhance the controller's performance. For instance, a study introduced an extended Kalman filter to enhance the control system of a USV (Wang et al., 2019). In some cases, the dynamic model is used for position estimation. Subsys-

tem failures in sensors and control equipment can potentially lead to a considerable loss of motion control. Therefore, the control system should be robust during potential failures (Wan et al., 2022).

Most studies have predominantly focused on the development of advanced path-following systems for small USVs. However, a noticeable gap in research concerning relatively large commercial vessels exists; this issue has been overlooked in previous investigations. Despite the abundance of studies on control, the impact of loading conditions on path-following systems for displacement vessels has yet to be explored. This study aims to enhance the performance of path-following control for underactuated displacement vessels, considering various loading conditions, such as ballast, full load, and other relevant scenarios. The L1 adaptive control (model reference) structure, which effectively mitigates the adverse effects of different loading conditions on path-following control, was used to address this gap. Simulations were conducted at full-scale, incorporating challenging environmental factors, such as heavy sea waves, currents, and wind.

2 Equations of vessel motions

For motion description, two coordinate systems were defined in Figure 1. The Fossen dynamic model was utilized to describe the vessel's motion and estimate the forces and moments acting on the hull (Fossen, 2002). The model considered three degrees of freedom: surge, sway, and yaw, ignoring heave, roll, and pitch because of their minor importance. The ship was considered a rigid body in the vessel's center of gravity. Equation (1) represents the positions, velocities, and forces in these degrees of freedom.

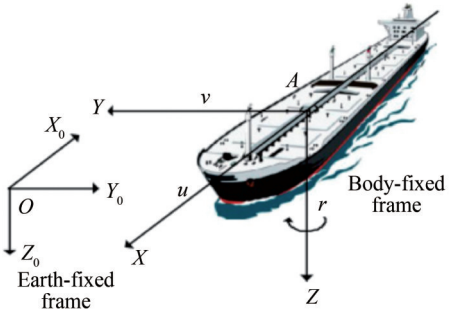

Figure 1 Earth-fixed and body-fixed frames (Fossen, 2002)

$$\begin{aligned} \boldsymbol{\eta} &= [\, x, y, \psi \,]^{\mathrm{T}} \\ \boldsymbol{v} &= [\, u, v, r \,]^{\mathrm{T}} \\ \boldsymbol{\tau} &= [\, X, Y, N \,]^{\mathrm{T}} \end{aligned} \tag{1}$$

where $\boldsymbol{\eta}$ is the position and rotation in the Earth-fixed frame, $\boldsymbol{v}$ represents the linear and angular velocity vector, and $\boldsymbol{\tau}$ indicates the forces and moments acting on the hull. Fossen introduced a conventional model widely used for displacement vehicles (Moreira et al., 2007; Do et al., 2004; Zheng and Sun, 2016), as indicated in Equation (2) (Fossen, 2002).

$$\left(\boldsymbol{M}_{\mathrm{RB}} + \boldsymbol{M}_{A}\right)\dot{v} + \boldsymbol{C}(v)v + \boldsymbol{D}_{d}v = \boldsymbol{\tau}_{\mathrm{rudder}} + \boldsymbol{\tau}_{\mathrm{propeller}} + \boldsymbol{\tau}_{\mathrm{ext}} \tag{2}$$

Equation (2) includes the external $\left(\boldsymbol{\tau}_{\mathrm{ext}}\right)$, the propeller $\left(\boldsymbol{\tau}_{\mathrm{propeller}}\right)$, the rudder $\left(\boldsymbol{\tau}_{\mathrm{rudder}}\right)$, the hydrodynamic damping $\left(\boldsymbol{D}_{d}\right)$, the rigid body $\left(\boldsymbol{M}_{\mathrm{RB}}\right)$, added mass $\left(\boldsymbol{M}_{A}\right)$, and Coriolis and centripetal $(\boldsymbol{C})$ terms.

$$\boldsymbol{\tau}_{\mathrm{ext}} = \boldsymbol{\tau}_{\mathrm{wind}} + \boldsymbol{\tau}_{\mathrm{current}} + \boldsymbol{\tau}_{\mathrm{wave}} \tag{3}$$

The rigid body equation is expressed as follows:

$$\boldsymbol{M}_{\mathrm{RB}} = \begin{bmatrix} m & 0 & 0 \\ 0 & m & mx_g \\ 0 & mx_g & I_z \end{bmatrix} \tag{4}$$

Displacement vessels generally transit within a low-speed range ($Fn < 0.3$). Consequently, first-order derivatives of hydrodynamic coefficients offer sufficient accuracy. Linear hydrodynamic coefficients are the most important vessel behavior, and higher-order derivatives have been ignored. The added mass terms are presented in Equation (5) as follows:

$$\boldsymbol{M}_{A} = \begin{bmatrix} X_{\dot{u}} & 0 & 0 \\ 0 & Y_{\dot{v}} & 0 \\ 0 & 0 & N_{\dot{r}} \end{bmatrix} \tag{5}$$

When a vessel moves through a fluid, it experiences pressure and shear drag. The hydrodynamic damping terms for the displacement vessel are vital factors affecting the vessel's dynamics, as outlined in the following equation:

$$\boldsymbol{D}_{d} = \begin{bmatrix} X_{u} & 0 & 0 \\ 0 & Y_{v} & Y_{r} \\ 0 & N_{v} & N_{r} \end{bmatrix} \tag{6}$$

The Coriolis effect and centripetal force are expressed as follows:

$$\boldsymbol{C}(v) = \begin{bmatrix} 0 & 0 & -m\left(v + x_g r\right) + Y_{\dot{v}} v \\ 0 & 0 & \left(m - X_{\dot{u}}\right)u \\ m\left(v + x_g r\right) - Y_{\dot{v}} v & -\left(m - X_{\dot{u}}\right)u & 0 \end{bmatrix} \tag{7}$$

The rudder and propeller effects are modeled as follows:

$$\boldsymbol{\tau}_{\text{propeller}} = \begin{bmatrix} K_T \rho n^2 {D_P}^4 \\ 0 \\ 0 \end{bmatrix} \tag{8}$$

$$\boldsymbol{\tau}_{\text{rudder}} = \delta \begin{bmatrix} 0 \\ \frac{1}{2}\rho C_L A u^2 \\ \frac{1}{2}\rho C_L A u^2 x_r \end{bmatrix} \tag{9}$$

2.1 Ocean disturbances

Waves, currents, and wind are prominent ocean disturbances that greatly challenge maritime vehicles. These disturbances are consistently present in the marine environment and influence maritime vehicles considerably. Waves, for instance, can deflect the vessel from the desired position. Given that waves are common in the sea, their effects must be considered when designing a path-following control system, as depicted in Equation (10) (Fossen, 2002).

$$\boldsymbol{\tau}_{\text{wave}} = \boldsymbol{\tau}_{\text{wave1}} + \boldsymbol{\tau}_{\text{wave2}} \tag{10}$$

The forces and moments induced by waves depend on wave frequency, vessel speed, angle of encounter, and wave height. Wind also contributes to external forces and moments. Equation (11) models the forces and moments caused by wind.

$$\boldsymbol{\tau}_{\text{wind}} = \frac{1}{2}\rho_a V_{\text{rw}}^2 \begin{bmatrix} C_X(\gamma_{\text{rw}}) A_{\text{Fw}} \\ C_y(\gamma_{\text{rw}}) A_{\text{Lw}} \\ C_N(\gamma_{\text{rw}}) A_{\text{Lw}} L_{\text{oa}} \end{bmatrix} \tag{11}$$

The coefficients of wind forces and moments are dependent on the wind angle of attack, denoted by γ_{rw}. Then, γ_{rw} represents the wind angle of attack relative to the vessel. Relative velocities between the vessel and the ocean current were considered to determine the impact of ocean currents.

$$u_r = u - u_c, v_r = v - v_c \tag{12}$$

2.2 Calculation of hydrodynamic coefficients

Various loading conditions in displacement vessels change their dynamic behavior. The control system is designed based on the dynamic model and performance of the system. A major factor influencing the dynamic behavior of commercial vessels is draught variation, which significantly alters parameters such as mass, inertia, and hydrodynamic coefficients. The VLCC2 oil tanker, a benchmark vessel, has been selected as a case study for modeling and motion control design. Its specifications are detailed in Table 1. Hydrodynamic coefficients were calculated for full load and ballast conditions using empirical formulas in Tables 2 and 3. The VLCC2, similar to many conventional commercial displacement vessels, is an underactuated vessel. It is equipped with a propeller for propulsion and a rudder for steering. Full load and ballast conditions for commercial vessels are commonly different. These loading conditions cause considerable changes in the vessel's draught, mass, and inertia. Table 1 presents the geometrical characteristics under full load and ballast conditions.

Table 1 VLCC2 vessel main characteristics

Parameter	Full load	Ballast
Fn	0.141	0.141
L (m)	320	320
B (m)	58	45.7
D (m)	20.8	10.1
∇ (m^3)	312 600	109 300
x_g (m)	11.2	11.2
I_z (m)	2.05×10^{12}	7.17×10^{11}
C_B	0.81	0.74
D_P (m)	9.86	9.86
x_r (m)	176	176
A (m^2)	112.5	112.5
Scale	1	1

Table 4 presents the hydrodynamic coefficients of the VLCC2 vessel under the ballast and full load conditions. The table emphasizes that the coefficients and inertia parameters, such as mass, vary significantly between ballast and full load conditions. Consequently, when designing the control system, a robust controller for the full load condition may not necessarily be as effective for the ballast condition.

3 Adaptive path-following control

The loading conditions directly affect the dynamic behavior; that is, accelerations and velocities are influenced by these loading conditions. The adaptive law technique used in this study predicts the dynamic behavior of the vessel by the state estimator. The state estimator predicts the effect of unmodeled parameters, thereby determining the control gains. These gains must be adjusted to improve the performance of the path-following control relative to the fixed structure.

The waypoint with navigation function often generates the reference path to guide the ship in maritime navigation (Zhang and Zhang, 2013). In this study, the path-following control generated commands to guide the vessel to the desired position. The guidance system that uses the LOS technique sets the desired controller states. Then, the controller attempted to reach the desired state using naviga-

Table 2 Empirical formulas for the hull's added mass coefficients

References	Equation	unit
Clarke et al. (1983)	$X_{\dot{u}} = 0.05m$	kg
Zhou et al. (1983)	$Y_{\dot{v}} = m\left[0.882 - 0.54C_B\left(1 - 1.6\frac{D}{B}\right) - 0.156\left(1 - 0.673C_B\right)\frac{L}{B} + 0.826\frac{D}{B}\frac{L}{B}\left(1 - 0.678\frac{D}{B}\right) - 0.638C_B\frac{D}{B}\frac{L}{B}\left(1 - 0.669\frac{D}{B}\right)\right]$	kg
Zhou et al. (1983)	$N_{\dot{r}} = m\left[\frac{1}{100}\left(33 - 76.85C_B\left(1 - 0.784C_B\right) + 3.43\frac{L}{B}\left(1 - 0.63C_B\right)\right)\right]$	kg·s^2

Table 3 Empirical formulas for the hull's damping coefficients

References	Equation	unit
Yasukawa and Yoshimura (2015)	$X_u = -0.011\rho LDU$	kg/s
Lee (1998)	$Y_v = \left(\left[-0.4545\frac{D}{L} + 0.065C_B\frac{B}{L}\right]\frac{L}{D}\right)\cdot\frac{1}{2}\rho LDU^2$	kg/s
	$Y_r = \left(\left[-0.115C_B\frac{B}{L} + 0.0024\right]\frac{L}{D}\right)\cdot\frac{1}{2}\rho LDU^2$	kg·m/s
	$N_v = x_g Y_v$	kg·m/s
	$N_r = \left(\left[-0.003\,724 + 0.104\,46\frac{D}{L} - 1.393\left(\frac{D}{L}\right)^2\right]\frac{L}{D}\right)\cdot\frac{1}{2}\rho L^2 DU^2$	kg·m^2/s

Table 4 Hydrodynamic coefficients of the VLCC2 vessel for full load and ballast conditions

Parameter	Full load	Ballast
$X_{\dot{u}}$ (kg)	1.60×10^7	5.60×10^6
$Y_{\dot{v}}$ (kg)	2.45×10^8	6.04×10^7
$N_{\dot{r}}$ (kg·s^2)	1.22×10^7	5.39×10^6
X_u (kg/s)	-5.97×10^5	-2.89×10^5
Y_v (kg/s)	-6.64×10^7	-2.48×10^7
Y_r (kg·m/s)	-4.81×10^8	-3.24×10^7
N_v (kg·m/s)	-9.62×10^9	-1.44×10^9
N_r (kg·m^2/s)	-1.95×10^8	-6.09×10^7

tion feedback. The interceptor is intended to accomplish an intercept by limiting its motion along the LOS vector between the reference point and the target. The schematic of the proposed adaptive path-following control structure is depicted in Figure 2.

3.1 L1 adaptive control for heading angle

The L1 adaptive controller is a suitable adaptive control structure developed for systems with unknown parameters, disturbances, and time-varying parameters (Hovakimyan et al., 2011). The main structure for this type of controller is shown in Equation (13).

$$\begin{aligned}\dot{\boldsymbol{x}}_s(t) &= \boldsymbol{A}_m\boldsymbol{x}_s(t) + \boldsymbol{B}_m\left(\omega\delta(t) + \theta^{\mathrm{T}}(t)\boldsymbol{x}_s + \sigma(t)\right)\\ y_s(t) &= c^{\mathrm{T}}\boldsymbol{x}_s(t)\end{aligned} \tag{13}$$

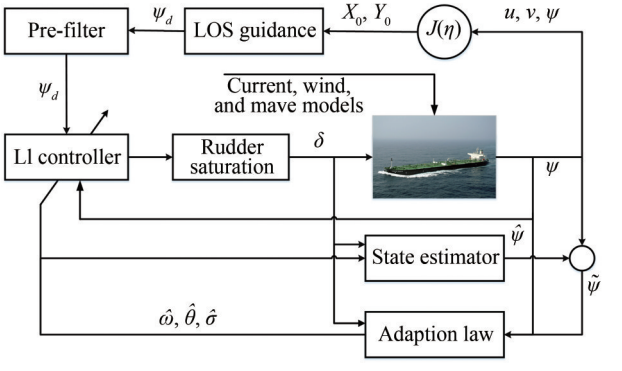

Figure 2 Schematic of the proposed adaptive path-following control structure

All unknown parameters in Equation (13) were considered bounded parameters. The reference model for the yaw motion was defined in Equation (14).

$$\underbrace{\begin{bmatrix}\dot{\psi}\\ \dot{r}\end{bmatrix}}_{\dot{x}_s} = \underbrace{\begin{bmatrix}0 & 1\\ 0 & \frac{N_r}{I_Z + N_{\dot{r}}}\end{bmatrix}}_{A_m}\underbrace{\begin{bmatrix}\psi\\ r\end{bmatrix}}_{x_s} + \underbrace{\begin{bmatrix}0\\ \frac{0.5\rho C_L U^2 A x_r}{I_Z + N_{\dot{r}}}\end{bmatrix}}_{B_m}\delta \tag{14}$$

The yaw reference model (14) is considered for pursuing the desired yaw. This reference model generates the continuous output $\hat{y}_s(t)$ using the desired yaw $\psi_d(t)$. To predict the yaw of the vessel, the estimated unknown parameters are integrated in Equation (14).

$$\begin{aligned}\dot{\hat{\boldsymbol{x}}}_s(t) &= \boldsymbol{A}_m\boldsymbol{x}_s(t) + \boldsymbol{B}_m\left(\hat{\omega}\delta(t) + \hat{\theta}^{\mathrm{T}}(t)x_s + \hat{\sigma}(t)\right)\\ \hat{y}_s(t) &= \boldsymbol{c}^{\mathrm{T}}\hat{\boldsymbol{x}}_s(t)\end{aligned} \tag{15}$$

where $\hat{\boldsymbol{x}}_s \in R^{n\times 1}$ indicates the state estimation. Equation (15) depicts the structure of the estimator. The estimator used the control signal and the system output to estimate the states for the next step. The adaptation laws were applied to approximate the unknown parameters, achieving improved performance. The unknown parameters are assessed using Equation (16).

$$\begin{aligned}\dot{\hat{\omega}}(t) &= \Gamma\mathrm{proj}\left(\hat{\omega}(t), -u(t)\tilde{\boldsymbol{x}}_s^{\mathrm{T}}(t)\boldsymbol{P}\boldsymbol{B}_m\right),\ \hat{\omega}(0) = \hat{\omega}_0\\ \dot{\hat{\theta}}(t) &= \Gamma\mathrm{proj}\left(\hat{\theta}(t), -x(t)\tilde{\boldsymbol{x}}_s^{\mathrm{T}}(t)\boldsymbol{P}\boldsymbol{B}_m\right),\ \hat{\theta}(0) = \hat{\theta}_0\\ \dot{\hat{\sigma}}(t) &= \Gamma\mathrm{proj}\left(\hat{\sigma}(t), -\tilde{\boldsymbol{x}}_s^{\mathrm{T}}(t)\boldsymbol{P}\boldsymbol{B}_m\right),\ \hat{\sigma}(0) = \hat{\sigma}_0\end{aligned} \tag{16}$$

where $\Gamma \in (0,\infty)$ is the adaptation rate; $\boldsymbol{P} = \boldsymbol{P}^{\mathrm{T}} > 0$ indicates the positive definite matrix, which is extracted from the Lyapunov equation $\boldsymbol{A}_m^{\mathrm{T}}\boldsymbol{P} + \boldsymbol{P}\boldsymbol{A}_m = -\boldsymbol{Q}$, and $\tilde{\boldsymbol{x}}_s = \hat{\boldsymbol{x}}_s - \boldsymbol{x}_s$ defined as the prediction error. Finally, the projection operation is expressed in Equation (17) (Hovakimyan et al., 2011).

$$\mathrm{proj}(\theta, y) \cong \begin{cases} y & \text{if } f(\theta) < 0\\ y & \text{if } f(\theta) \geqslant 0 \text{ and } \nabla f^{\mathrm{T}} y \leqslant 0\\ y - \dfrac{\nabla f}{\|\nabla f\|}\left\langle \dfrac{\nabla f}{\|\nabla f\|}, y\right\rangle f(\theta) & \text{if } f(\theta) \geqslant 0 \text{ and } \nabla f^{\mathrm{T}} y > 0\end{cases} \tag{17}$$

The projection operator in the adaptation laws attempted to estimate the parameters to prevent diverging because function Y is bounded (Patre et al., 2008). The projection function was used in many common adaptive controllers to ensure the robustness of the adaptation law, validating the stability of the internal signals within the system.

Asymptotic convergence of the error signal was determined using Barbalat's lemma, which enhanced the adaptive controller using the adaptation law approach in the upcoming subsection (Dydek et al., 2010; Lavretsky and Wise, 2012). The L1 controller signal law for the vessel's heading is obtained using Equation (18) (Hovakimyan et al., 2011).

$$\delta(t) = \frac{1}{\hat{\omega}(t)}\left(k_g\psi_d(t) - \hat{\theta}^{\mathrm{T}}(t)\boldsymbol{x}_s - \hat{\sigma}(t)\right) \tag{18}$$

where k_g is computed using $k_g = -1/\left(\boldsymbol{c}^{\mathrm{T}}\boldsymbol{A}_m^{-1}\boldsymbol{B}_m\right)$.

3.2 Stability analysis

The bounds and asymptotic properties of the error are examined using the Lyapunov-function candidate (19).

$$\begin{aligned}V\left(\tilde{\boldsymbol{x}}_s(t), \tilde{\omega}(t), \tilde{\theta}(t), \tilde{\sigma}(t)\right) =\\ \boldsymbol{x}_s^{\mathrm{T}}(t)\boldsymbol{P}\tilde{\boldsymbol{x}}_s(t) + \frac{1}{\Gamma}\left(\tilde{\omega}^2(t), \tilde{\theta}^{\mathrm{T}}(t)\tilde{\theta}(t), \tilde{\sigma}^2(t)\right)\end{aligned} \tag{19}$$

A derivative of (19), along with the estimation error (20), derives Equation (21) as follows:

$$\dot{\tilde{\boldsymbol{x}}}_s(t) = \boldsymbol{A}_m\tilde{\boldsymbol{x}}_s(t) + \boldsymbol{B}_m\left(\tilde{\omega}(t)\delta(t) + \tilde{\theta}^{\mathrm{T}}(t)\boldsymbol{x}_s(t) + \tilde{\sigma}(t)\right) \tag{20}$$

$$\begin{aligned}\dot{V}(t) &= \tilde{\boldsymbol{x}}_s^{\mathrm{T}}(t)\left(\boldsymbol{A}_m^{\mathrm{T}}\boldsymbol{P} + \boldsymbol{P}\boldsymbol{A}_m\right)\tilde{\boldsymbol{x}}_s(t)\\ &+2\tilde{\boldsymbol{x}}_s^{\mathrm{T}}(t)\boldsymbol{P}\boldsymbol{B}_m\left(\tilde{\sigma}(t) + \tilde{\omega}(t)\delta(t) - \tilde{\theta}^{\mathrm{T}}(t)\tilde{\boldsymbol{x}}_s(t)\right)\\ &+\frac{2}{\Gamma}\left(\dot{\hat{\omega}}(t)\tilde{\omega}(t) + \dot{\hat{\theta}}(t)\tilde{\theta}(t) + \dot{\hat{\sigma}}(t)\tilde{\sigma}(t)\right)\\ &-\frac{2}{\Gamma}\left(\tilde{\sigma}(t)\dot{\sigma}(t) + \tilde{\theta}(t)\dot{\theta}(t)\right)\end{aligned} \tag{21}$$

Then,

$$\begin{aligned}\dot{V}(t) &= -\tilde{\boldsymbol{x}}_s^{\mathrm{T}}(t)\boldsymbol{Q}\tilde{\boldsymbol{x}}_s(t)\\ &+2\tilde{\omega}(t)\left(\tilde{\boldsymbol{x}}_s^{\mathrm{T}}(t)\boldsymbol{P}\boldsymbol{B}_m\delta(t) + \mathrm{proj}\left(\hat{\omega}(t), \delta(t)\tilde{\boldsymbol{x}}_s^{\mathrm{T}}(t)\boldsymbol{P}\boldsymbol{B}_m\right)\right)\\ &+2\tilde{\theta}(t)\left(\tilde{\boldsymbol{x}}_s^{\mathrm{T}}(t)\boldsymbol{P}\boldsymbol{B}_m\boldsymbol{x}_s(t) + \mathrm{proj}\left(\hat{\theta}(t), -\boldsymbol{x}_s(t)\tilde{\boldsymbol{x}}_s^{\mathrm{T}}(t)\boldsymbol{P}\boldsymbol{B}_m\right)\right)\\ &-2\tilde{\sigma}(t)\left(\tilde{\boldsymbol{x}}_s^{\mathrm{T}}(t)\boldsymbol{P}\boldsymbol{B}_m - \mathrm{proj}\left(\hat{\sigma}(t), \tilde{\boldsymbol{x}}_s^{\mathrm{T}}(t)\boldsymbol{P}\boldsymbol{B}_m\right)\right)\\ &-\frac{2}{\Gamma}\left(\tilde{\sigma}(t)\dot{\sigma}(t) + \tilde{\theta}(t)\dot{\theta}(t)\right)\end{aligned} \tag{22}$$

Notice that $\dot{V}(t) \leqslant 0$, if

$$\|\tilde{\boldsymbol{x}}_s(t)\| \leqslant \frac{\gamma_0}{\sqrt{\Gamma'}} \quad \text{for all } t \geqslant 0 \tag{23}$$

where $\theta_{\max} \cong \max_{\theta\in\Theta}\|\theta\|$, and for γ_0

$$\begin{aligned}\gamma_0 &\cong \sqrt{\frac{\theta_{mi}}{\lambda_{\min}(P)'}}\\ \theta_{mi} &\cong 4\theta_{\max}^2 + 4\sigma_b^2 + \left(\omega_{\max} - \omega_{\min}\right)^2\\ &+\frac{4\lambda_{\max}(P)}{\lambda_{\min}(Q)}\left(\theta_{\max}d_\theta + \sigma_b d_\sigma\right)\end{aligned} \tag{24}$$

Equations (19) and (21) are independent of the control signal. Consequently, the estimation error is independent of the control signal. Over time, the state predictor with the control signal (18) is equivalent to the reference model (14). $\boldsymbol{x}_s$ is bounded because $\hat{\boldsymbol{x}}_s$ and $\tilde{\boldsymbol{x}}_s$ are uniformly bounded (Hovakimyan et al., 2011).

3.3 Rudder constraints

The actuator may be involved in constraints that limit its ability to apply the control command. Conventional vessel rudders face two main constraints: the maximum deflection rate and the maximum/minimum deflection angles. Typically, rudder deflection for commercial vessels is confined within the range of −35° to 35°, and the maximum deflection rate is limited to 2.3(°)/s. Equation (25) was utilized to determine the rudder's deflection rate, whereas Equation (26) was used to identify the maximum and minimum deflection angle constraints.

$$\dot{\delta}_{\min} \leqslant \dot{\delta}(t) \leqslant \dot{\delta}_{\max} \tag{25}$$

$$\delta_{\min} \leqslant \delta(t) \leqslant \delta_{\max} \tag{26}$$

4 Results and discussion

In the previous sections, we discussed the dynamic model, hydrodynamic coefficients, and adaptive path-following control structure. This section focused on the simulation of the following predefined paths for VLCC2 based on the LOS guidance. The adaptive structure and the fixed structure were compared; the results showed that the only difference in the path-following control was the controller's structure.

For the PID controller, control gains (k_p, k_i, and k_d) for the yaw angle were set to 0.61, 0.000 105, and 1.74, respectively. These values were calculated using the hydrodynamic coefficients, natural frequency, and the rudder saturation under the full load condition (Fossen, 2002). On the contrary, in the L1 adaptive controller, the initial values of $\hat{\omega}_0, \hat{\theta}_0, \hat{\sigma}_0$ were set to 1, 0, and 0, respectively. Moreover, the adaptive rate was denoted as $\Gamma = 0.1$. Full load and ballast conditions under ocean disturbances were examined separately.

4.1 Simulation results of full load condition

In this state, the path-following control guided the VLCC2 to remain on the desired path using the PID and L1 adaptive controllers. At the onset of the simulation, the guidance system determined the desired heading for the control system based on the initial positions. In the next step, using the control algorithm, the controller decides the rudders deflection. The dynamic model represented the vessel's motions to estimate the next time step movement. The guidance system and the described cycle were repeated based on the new position until the final waypoint. The simulations were conducted using the hydrodynamic coefficients for the full load and full-scale condition. The desired positions are presented in Table 5.

Table 5 Desired waypoints

Desired waypoints	X_0 (km)	Y_0 (km)
Initial position	0	0
Waypoint 1	0	10
Waypoint 2	5	10
Waypoint 3	5	−10
Waypoint 4	10	−10
Waypoint 5	10	10
Waypoint 6	15	10
Waypoint 7	15	0

Figure 3 depicts the trajectory of the vessel under PID and L1 controllers. In this scenario, the classical and adaptive controllers exhibited excellent performance. The heading error and velocities for both cases were relatively close to each other (Figures 4 and 5), causing a similar control command in these scenarios. Figure 6 demonstrates the estimated parameters by the adaptation law for the adaptive control. These parameters were bounded and indicated that the estimation performance was accurate. The RMSE of the tracking errors must be analyzed, and the performance of the two controllers must be compared (Table 6). The comparison of the results in Table 6 indicates that the error value and performance of the two controllers are close. Consequently, for the dynamics with specified parameters, advanced controllers may not be used.

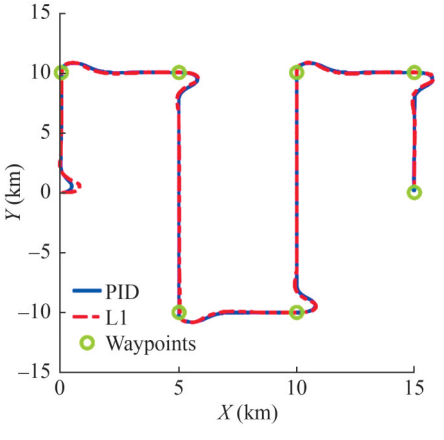

Figure 3 Trajectory of the vessel for full load condition

4.2 Simulation results of ballast condition

Commercial vessels frequently transition between ports

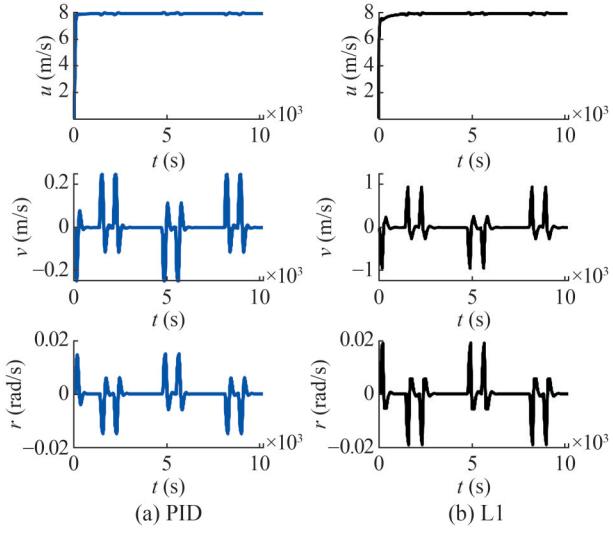

Figure 4 Linear and angular velocities for full load condition

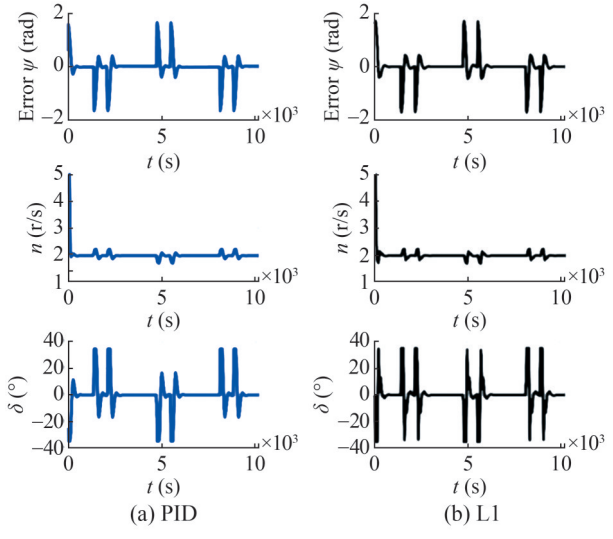

Figure 5 Heading error, propeller rotation, and rudder angle curve for full load

under varying loading conditions. Path-following control systems must track the path under any loading conditions. Simulations were conducted using hydrodynamic coefficients for the ballast condition and at full scale to assess the impact of loading conditions. The objective was to track desired positions, as presented in Table 5.

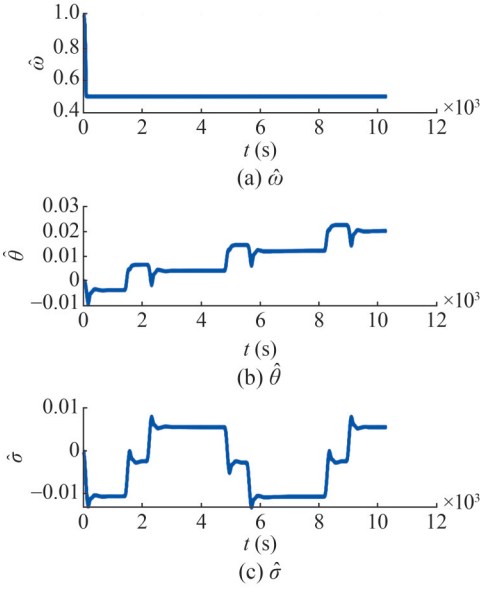

Figure 6 Estimated unknown parameters for full load condition

Figures 7 and 8 demonstrate the trajectory and velocities of the vessel. Notably, the performance of the classical PID controller in the ballast condition decreased compared with that of the full load condition. The trajectory plot (Figure 8) reveals oscillations around the interceptor for the PID controller case. Furthermore, the speed and control commands (Figures 8 and 9) indicated significant oscillations compared with the L1 adaptive controller. The PID controller's robustness decreased because it could not adapt its gains effectively. On the contrary, the L1 controller (Figure 10) exhibited robustness and excellent performance despite the changes in the dynamic behavior. The L1 controller used an adaptation law to estimate unknown parameters (Figure 11) that minimized the impact of uncertainty and unmodeled parameters in path-following control. As a result, estimating unknown parameters enhanced the performance of the proposed approach. Table 6 illustrates the RSME of the tracking error for the yaw angle, indicating that the adaptive control structure had a smaller error and rudder usage cost function than the traditional controller.

Table 6 RMSE of tracking error and rudder usage cost function

Condition	Controller	RMSE ψ (°)	RMSE ψ_m (°)	$\sum\left\lvert \Delta t\left(\delta_i - \delta_{i-1}\right)\right\rvert$
Full load	PID	0.079	–	1.24
	L1	0.072	0.024	1.27
Ballast	PID	0.059	–	3.45
	L1	0.068	0.007	1.4
Full load under disturbances	PID	–	–	–
	L1	0.06	0.002	9.91

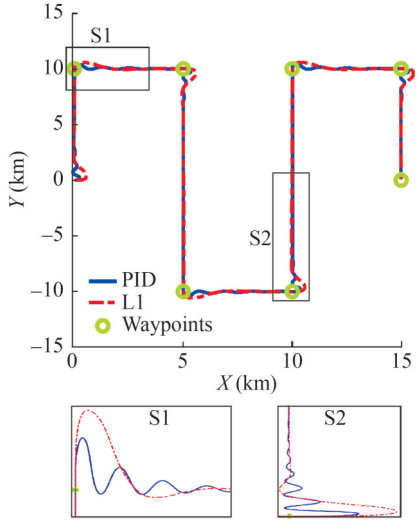

Figure 7 Trajectory of the vessel for ballast condition

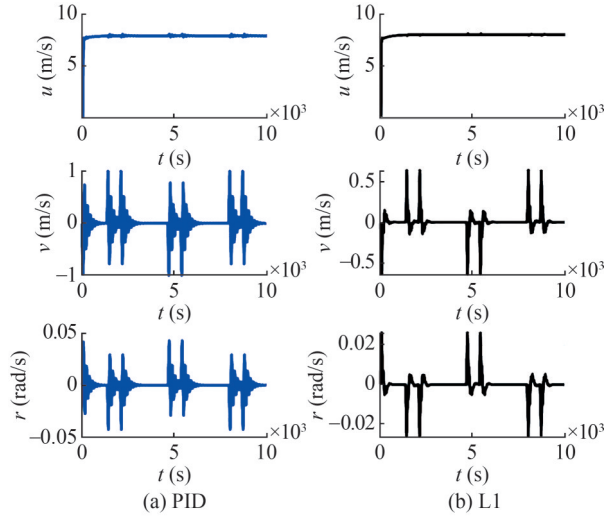

Figure 8 Linear and angular velocities for ballast condition

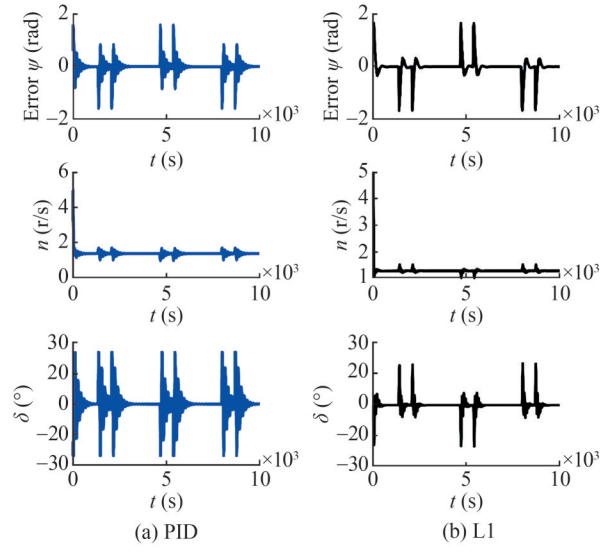

Figure 9 Heading error, propeller rotation, and rudder angle curve for ballast condition

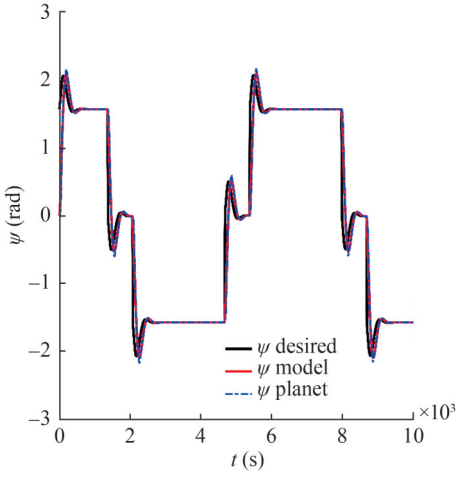

Figure 10 Yaw angle of desired, model reference, and planet (vessel) for ballast condition

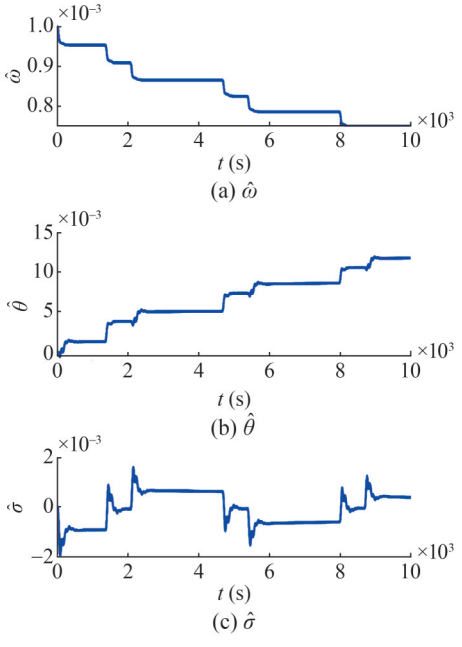

Figure 11 Estimated unknown parameters for ballast condition

4.3 Full load condition under ocean disturbances

In this section, the two designated controllers for full load and full-scale conditions under disturbances are used to track the desired path. The controllers attempted to reach the desired yaw angle of the vessel at each time step. The simulation's initial point was set at the origin of the Earth-fixed frame.

The performance of the controllers in the presence of ocean disturbances was evaluated. The simulations involved ocean conditions of sea state 5 with a frequency of 0.1 (T= 62.8 s). A two-knot current and a two-knot wind blowing were also observed at a 45° angle to the north. These conditions were applied to the vessel throughout the simulation.

In the simulations described in Section 4.3, the effect of

ocean disturbances was continually applied to the vessel's hull. The waves periodically influenced the vessel's three degrees of freedom, depending on the encounter angle and encounter frequency. Figure 12 shows that the trajectory that inferred the vessel with the classical controller could not track the desired path, whereas the L1 adaptive controller demonstrated excellent performance. Figure 13 illustrates the velocities during the path-following in the presence of disturbances. Moreover, the hull had a drift angle (sway velocity) due to currents and winds. Wave forces induced motion oscillations, resulting in fluctuations of control commands (Figure 14). The L1 controller attempted to bring the vessel output closer to the reference model (Figure 15) by estimating unknown parameters (Figure 16). Remarkably, in the presence of disturbances, the L1 controller has demonstrated excellent and high-quality path-following performance, whereas the classical controller was disabled to track the desired position.

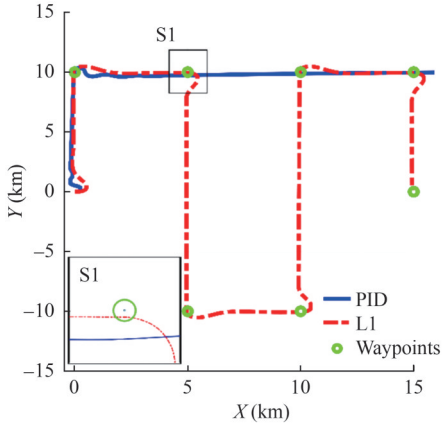

Figure 12 Trajectory of the vessel for full load condition under disturbances

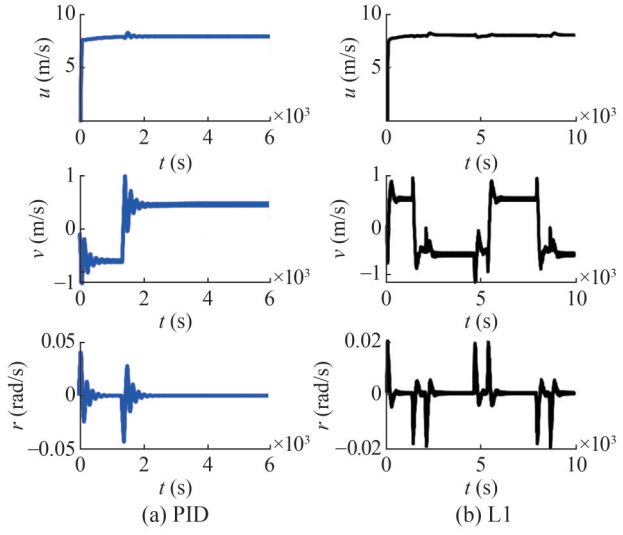

Figure 13 Linear and angular velocities for full load under disturbances

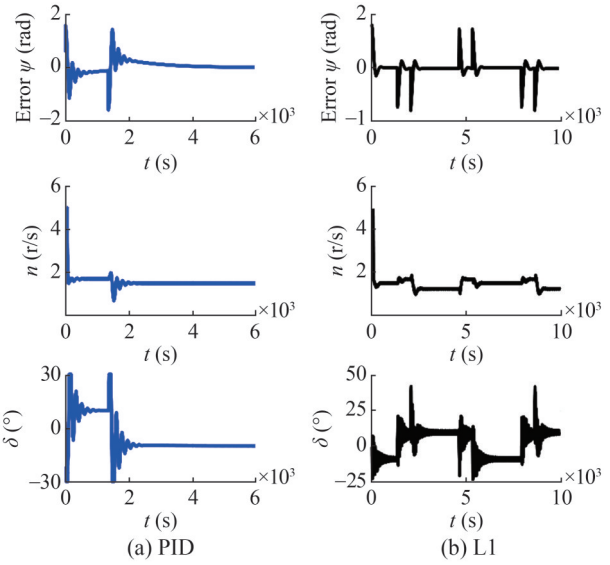

Figure 14 Heading error, propeller rotation, and rudder angle curve for full load under disturbances

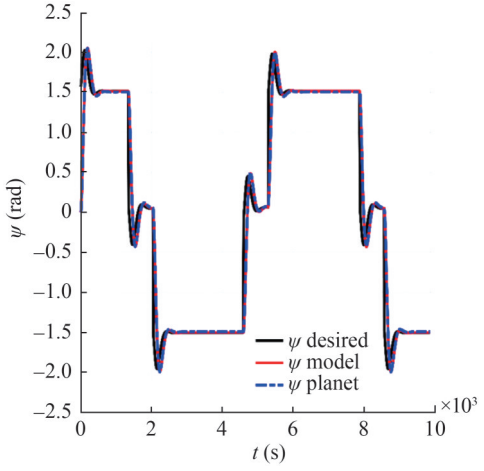

Figure 15 Yaw angle of desired, model reference, and planet (vessel) for full load condition under disturbances

Figure 18 shows the heading of the vessel during the path-following under the influence of disturbance forces and moments (Figure 17). A drift angle relative to the interceptor has been found due to external forces along the vessel's sway direction. This finding implies that the rudder was consistently deflected during the mission to overcome disturbances. Notably, when the vessel encountered quartering seas, the greatest deviation in heading occurred, whereas the slightest deviation occurred in the following and head seas (Figure 14).

Displacement vessels commonly transition within the harbors, and intelligent path-following control in similar situations requires performance assessment. Adaptive path-following control in the geography map has been evaluated to assess the performance of the two control systems. In this simulation, the vessel motioned under one-knot currents at a 3.92 m/s ($Fn = 0.07$) velocity, attempting to follow the

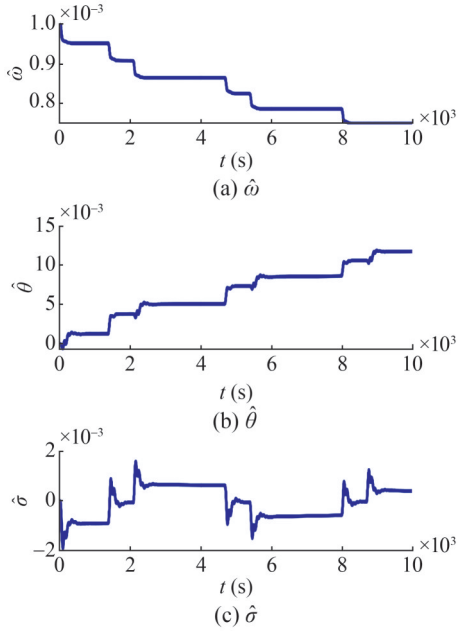

Figure 16 Estimated unknown parameters for full load condition under disturbances

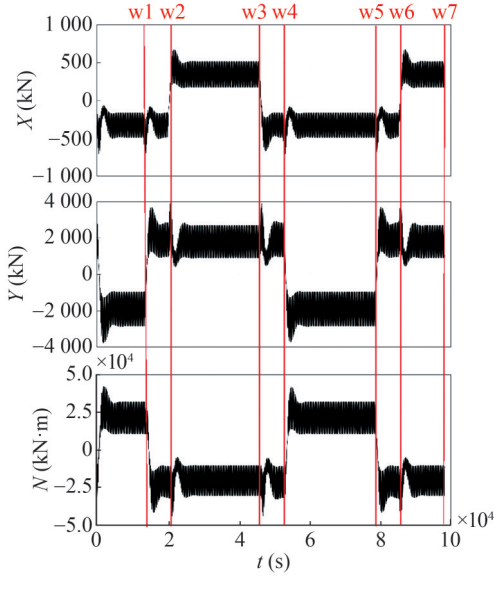

Figure 17 Disturbance forces and moment (waves, wind, and current)

position outlined in Table 7. The selected area for investigation was the harbor of Bandar-e-Imam Khomeini Port.

Figure 19 demonstrates the performance of the adaptive path-following control used for the VLCC2 vessel near Imam Khomeini Port. An overshoot was observed during the path-following process near waypoints due to the significant inertia and time delay. However, the L1 adaptive controller proved effective for maneuvering specific areas, such as harbors. On the contrary, the PID controller did not perform effectively in the following predefined paths, potentially leading to collision risk in a crowded area.

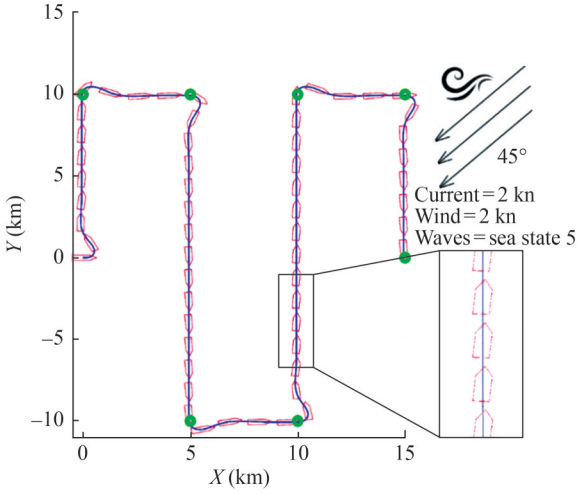

Figure 18 Hull's drift angle relative to the interceptor under disturbances

Table 7 Desired waypoints in geography map

Desired waypoints	Longitude	Latitude
Initial position	30.427 75	49.058 77
Waypoint 1	30.428 36	49.059 42
Waypoint 2	30.395 68	49.122 63
Waypoint 3	30.397 48	49.135 03
Waypoint 4	30.422 36	49.135 03
Waypoint 5	30.420 35	49.065 02

Figure 19 Trajectory of the vessel at the simulation of path-following in the geography map (Port of Bandar-e Emam Khomeyni)

5 Conclusion

An optimized path-following control enhances vessel guidance and system efficiency, reduces energy consumption, minimizes human intervention, and improves safety. It encompasses guidance, navigation, and control, where the performance of each component, particularly the controller, is essential and can extend the mission. An advanced controller for underactuated commercial vessels focused on path-following control was developed to improve control under various loading conditions and ocean disturbances, especially for displacement vessels. The L1 adaptive controller has been utilized to manage the states of commer-

cial tankers on the full scale. The findings indicate that linear and classical controllers (fixed structure) perform effectively under calm water and ideal environments. However, in other loading conditions, due to the changes in dynamic behavior, the classical controller exhibited poor performance and lost its capability under an uncertain environment. The L1 adaptive controller (adaptive structure), on the contrary, was robust due to the updated control gains at each time step through the estimation of unknown parameters. The adaptive control structure exhibited consistent performance even in uncertain environments. Notably, the L1 adaptive controller demonstrated robustness against significant draught changes. This finding highlights its potential to extend the operational range and enhance the performance of commercial vessels throughout the year.

Nomenclature

L	Length of vessel
D	Draught of vessel
C_B	Block coefficient of vessel
ρ	Water density
ρ_a	Air density
V_{rw}	Wind speed relative to vessel speed
L_{oa}	Longitudinal center of wind force from the center of gravity
X_0	x position in the Earth-fixed frame
Y_0	y position in the Earth-fixed frame
$\boldsymbol{\tau}_{\text{ext}}$	External forces and moment
U	Magnitude velocity
ψ	Yaw angle
u	Surge velocity
v	Sway velocity
r	Yaw rate
m	Vessel's mass
Fn	Froud number
I_Z	Mass moment of inertia around the Z-axis
X_u	Surge linear hydrodynamic damping with respect to surge velocity
Y_v	Sway linear hydrodynamic damping with respect to sway velocity
N_r	Yaw linear hydrodynamic damping with respect to yaw velocity
Y_r	Sway linear hydrodynamic damping with respect to yaw velocity
N_v	Yaw linear hydrodynamic damping with respect to sway velocity
u_c, v_c	Surge and sway velocities of current in body-fixed frame
u_r, v_r	Relative surge and sway velocities between current and vessel
$\dot{\delta}_{\max}, \dot{\delta}_{\min}$	Maximum and minimum rudder angle rate
$\delta_{\max}, \delta_{\min}$	Maximum and minimum rudder angle
ω, θ, σ	Unknown parameter, time variant unknown parameters and input disturbance
$\boldsymbol{P}$	Positive definite matrix
Γ	Adaptation rate
$\boldsymbol{c}$	Output matrix
V	Lyapunov-function candidate
$\hat{\boldsymbol{x}}_s$	Prediction state vector
$\tilde{\boldsymbol{x}}_s$	Prediction error of states vector
$\boldsymbol{Q}$	Positive and defined matrix
$\lambda_{\max}, \lambda_{\min}$	Max/min eigenvalue of the matrix
B	Beam of vessel
∇	Displacement of vessel
δ	Rudder angle
X, Y, N	Surge force, sway force, yaw moment around midship
C_X, C_Y, C_N	Surge force, sway force and yaw moment coefficients with respect to wind
γ_{rw}	Angle of attack of the wind relative to the vessel
$A_{\text{Fw}}, A_{\text{Lw}}$	Frontal and lateral projected areas above the water line
$\boldsymbol{M}_{\text{RB}}$	Rigid body term
$\boldsymbol{M}_A$	Added mass term
$\boldsymbol{C}$	Coriolis and centripetal matrix
D_d	Hydrodynamic damping term
D_P	Propeller diameter
K_T	Propeller thrust coefficient
n	Propeller rotational speed
x_g	Longitudinal center of gravity from midship
x_r	Longitudinal rudder from center of gravity
A	Rudder area
C_L	Rudder lift coefficient
$X_{\dot{u}}$	Surge linear added mass with respect to surge acceleration
$Y_{\dot{v}}$	Sway linear added mass with respect to sway acceleration
$N_{\dot{r}}$	Yaw linear added mass with respect to yaw acceleration
$\boldsymbol{\tau}_{\text{wave}}, \boldsymbol{\tau}_{\text{current}}, \boldsymbol{\tau}_{\text{wind}}$	Forces and moments of waves, current and wind acting on the hull
$\boldsymbol{\tau}_{\text{wave1}}$	First-order of the forces and moment of waves
$\boldsymbol{\tau}_{\text{wave2}}$	second-order of the forces and moment of waves
ψ_d	Desired yaw angle
k_p, k_i, k_d	Proportional, integral, and derivative gains of PID controller
$\boldsymbol{A}_m$	States matrix
$\boldsymbol{B}_m$	Actuator matrix

$\hat{\omega}, \hat{\theta}, \hat{\sigma}$	Estimated parameters of ω, θ, σ
$\hat{\psi}$	Prediction yaw angle
$\tilde{\psi}$	Prediction error of yaw angle
ψ_m	Yaw angle of the reference model
$\boldsymbol{x}_s$	State vector
y_s	Output vector
$\hat{y}_s$	Prediction output vector

Competing interest The authors have no competing interests to declare that are relevant to the content of this article.

References

Abril J, Salom J, Calvo O (1997) Fuzzy control of a sailboat. International Journal of Approximate Reasoning 16(3-4): 359-375. https://doi.org/10.1016/S0888-613X(96)00132-6

Annamalai AS, Sutton R, Yang C, Culverhouse P, Sharma S (2014) Innovative adaptive autopilot design for uninhabited surface vehicles. ISSC 2014/CIICT 2014. https://doi.org/10.1049/cp.2014.0677

Breivik M, Hovstein VE, Fossen TI (2008) Straight-line target tracking for unmanned surface vehicles. Modeling, Identification and Control (MIC), 131-149. DOI: 10.4173/mic.2008.4.2

Chen M, Ge SS, How BE, Choo YS (2012) Robust adaptive position mooring control for marine vessels. IEEE Transactions on Control Systems Technology 21(2): 395-409

Chowdhury MI, Schwartz DG (2022) USV obstacle avoidance using a novel local path planner and novel global path planner with r-PRM. 54th International Symposium on Robotics, 1-8

Clarke D, Gedling P, Hing G (1983) The application of manoeuvering criteria in hull design using linear theory. Naval Architect 125: 45-68

Ding F, Wu J, Wang Y (2013) Stabilization of an underactuated surface vessel based on adaptive sliding mode and backstepping control. Mathematical Problems in Engineering 2013: 324954. https://doi.org/10.1155/2013/324954

Do KD, Jiang ZP, Pan J (2004) Robust adaptive path following of underactuated ships. Automatica 40(6): 929-944. https://doi.org/10.1016/j.automatica.2004.01.021

Dydek ZT, Annaswamy AM, Lavretsky E (2010) Adaptive control and the NASA X-15-3 flight revisited. IEEE Contr. Sys. Mag, 30(3): 32-48

Faramin M, Goudarzi RH, Maleki A (2019) Track-keeping observer-based robust adaptive control of an unmanned surface vessel by applying a 4-DOF maneuvering model. Ocean Engineering 183: 11-23. https://doi.org/10.1016/j.oceaneng.2019.04.051

Feemster MG, Esposito JM (2011) Comprehensive framework for tracking control and thrust allocation for a highly overactuated autonomous surface vessel. Journal of Field Robotics 28(1): 80-100

Fossen TI (2002) Marine control systems: guidance, navigation, and control of ships, rigs and underwater vehicles. Marine Cybernetics, Trondheim

Hasanvand A, Hajivand A (2019) Investigating the effect of rudder profile on 6DOF ship turning performance. Applied Ocean Research 92: 101918. https://doi.org/10.1016/j.apor.2019.101918

Hasanvand A, Hajivand A, Ali NA (2021) Investigating the effect of rudder profile on 6DOF ship course-changing performance. Applied Ocean Research 117: 102944. https://doi.org/10.1016/j.apor.2021.102944

Hasanvand A, Seif MS (2023) Designing the way point tracking intelligent system for displacement vessels with considering nonlinear dynamics. Journal of Marine Engineering 19(38): 155-167

Hovakimyan N, Cao C, Kharisov E, Xargay E, Gregory IM (2011) L1 adaptive control for safety-critical systems. IEEE Control Systems Magazine 31(5): 54-104. https://doi.org/10.1109/MCS.2011.941961

Lavretsky E, Wise KA (2012) Robust adaptive control. In Robust and adaptive control: With aerospace applications. Springer London, 317-353. https://doi.org/10.1016/j.oceaneng.2020.107310

Lee HY (1998) The prediction of ship's manoeuvring performance in the initial design stage. Proceedings of the PRADS Practical Design of Ships and Other Floating Bodies Conference, Maritime Research Institute Netherlands, The Hague, 633-639

Lefeber E, Pettersen KY, Nijmeijer H (2003) Tracking control of an underactuated ship. IEEE Transactions on Control Systems Technology 11(1): 52-61

Leslie E, Flint S, Briggs HC, Anderson ML, Appel G, Konig S, Bowen N, Foster C, Ganesh P, Ramos H (2022) An unmanned system for persistent surveillance in GPS-denied environments. In AIAA SCITECH 2022 Forum, 0118

Liu C, Zou ZJ, Hou XR (2014a) Stabilization and tracking of underactuated surface vessels in random waves with fin based on adaptive hierarchical sliding mode technique. Asian Journal of Control 16(5): 1492-1500

Liu C, Zou ZJ, Yin JC (2014b) Path following and stabilization of underactuated surface vessels based on adaptive hierarchical sliding mode. Int. J. Innov. Comput. Inf. Control 10: 909-918

Liu Y, Li Z, Liu J (2023) Path following of under-actuated ships based on backstepping and predictive control method. Science Progress 106(3): 00368504231191407

Liu Z, Chu R (2020) Robust adaptive heading control for a surface vessel with drift angles. Ocean Engineering 205:107310

Liu Z, Zhang Y, Yu X, Yuan C (2016) Unmanned surface vehicles: An overview of developments and challenges. Annual Reviews in Control 41: 71-93

Majohr J, Buch T (2006) Modelling, simulation and control of an autonomous surface marine vehicle for surveying applications Measuring Dolphin MESSIN. IEE Control Engineering Series 69: 329

Moradi MH, Katebi MR (2001) Predictive PID control for ship autopilot design. IFAC Proceedings Volumes 34(7): 375-380

Moreira L, Fossen TI, Guedes Soares C (2007) Path following control system for a tanker ship model. Ocean Engineering 34(14-15): 2074-2085

Pan CZ, Lai XZ, Yang SX, Wu M (2013) An efficient neural network approach to tracking control of an autonomous surface vehicle with unknown dynamics. Expert Systems with Applications 40(5): 1629-1635

Pastore T, Djapic V (2010) Improving autonomy and control of autonomous surface vehicles in port protection and mine countermeasure scenarios. Journal of Field Robotics 27(6): 903-914

Patre PM, MacKunis W, Kaiser K, Dixon WE (2008) Asymptotic tracking for uncertain dynamic systems via a multilayer neural network feed forward and rise feedback control structure. IEEE Trans. Autom. Control 53(9): 2180-2185

Schnurr RE, Walker TR (2019) Marine transportation and energy use. Reference Module in Earth Systems and Environmental

Sciences: 1-9. https://doi.org/10.1016/B978-0-12-409548-9.09270-8
Sharma SK, Sutton R (2012) Modelling the yaw dynamics of an uninhabited surface vehicle for navigation and control systems design. Journal of Marine Engineering & Technology 11(3): 9-20
Sonnenburg CR, Woolsey CA (2013) Modeling, identification, and control of an unmanned surface vehicle. Journal of Field Robotics 30(3): 371-398
Švec P, Thakur A, Raboin E, Shah BC, Gupta SK (2014) Target following with motion prediction for unmanned surface vehicle operating in cluttered environments. Autonomous Robots 36: 383-405
Talha M, Asghar F, Kim SH (2017) Design of fuzzy tuned PID controller for anti-rolling gyro (ARG) stabilizer in ships. International Journal of Fuzzy Logic and Intelligent Systems 17(3): 210-220
Wan L, Cao Y, Sun Y, Qin H (2022) Fault-tolerant trajectory tracking control for unmanned surface vehicle with actuator faults based on a fast fixed-time system. ISA Transactions 130: 79-91
Wang Y, Chai S, Nguyen HD (2019) Unscented Kalman filter trained neural network control design for ship autopilot with experimental and numerical approaches. Applied Ocean Research 85: 162-172
Wang N, Gao Y, Zhao H, Ahn CK (2020) Reinforcement learning-based optimal tracking control of an unknown unmanned surface vehicle. IEEE Transactions on Neural Networks and Learning Systems 32(7): 3034-3045
Wang N, He H, Hou Y, Han B (2023) Model-free visual servo swarming of manned-unmanned surface vehicles with visibility maintenance and collision avoidance. IEEE Transactions on Intelligent Transportation Systems.
Wang N, Zhang Y, Ahn CK, Xu Q (2021) Autonomous pilot of unmanned surface vehicles: Bridging path planning and tracking. IEEE Transactions on Vehicular Technology 71(3): 2358-2374
Wondergem M, Lefeber E, Pettersen KY, Nijmeijer H (2010) Output feedback tracking of ships. IEEE Transactions on Control Systems Technology 19(2): 442-448
Yasukawa H, Yoshimura Y (2015) Introduction of MMG standard method for ship maneuvering predictions. Journal of Marine Science and Technology 20: 37-52
Yuh J, Marani G, Blidberg DR (2011) Applications of marine robotic vehicles. Intelligent Service Robotics 4: 221-231
Zhang G, Zhang X (2013) Concise robust adaptive path-following control of underactuated ships using DSC and MLP. IEEE Journal of Oceanic Engineering 39(4): 685-694
Zhang H, Zhang X, Cao T, Bu R (2022) Active disturbance rejection control for ship path following with Euler method. Ocean Engineering 247: 110516
Zhao H, Gao X, Zhang Y, Zhang X (2023) Nonlinear control of decarbonization path following underactuated ships. Ocean Engineering 272: 113784
Zhao Z, Liu Y, Zou T, Hong KS, Li HX (2022) Robust adaptive fault-tolerant control for a riser-vessel system with input hysteresis and time-varying output constraints. IEEE Transactions on Cybernetics 53(6): 3939-3950
Zheng Z, Sun L (2016) Path following control for marine surface vessel with uncertainties and input saturation. Neurocomputing 177: 158-167
Zhou Z, Yan S, Feng W (1983) Manoeuvring prediction of multiple-purpose cargo ships. Ship Eng. 6: 21-36